Electronic Supplementary Material (ESI) for Journal of Materials Chemistry A.

Supplementary Material

Platinum Group Metal-free NiMo Hydrogen Oxidation Catalysts: High Performance and Durability in Alkaline Exchange Membrane Fuel Cells

Sadia Kabir[1], K. Lemire[1], Kateryna Artyushkova[1], Aaron Roy[1], Madeleine Odgaard[2], Debbie Schlueter[2], Alexandr Oshchepkov[3,4,5], Antoine Bonnefont[3], Elena Savinova[3], Dinesh C. Sabarirajan[6], Pratiti Mandal[7], Ethan J. Crumlin[7], Iryna V. Zenyuk[6], Plamen Atanassov[1] and Alexey Serov[1]*

[1]Department of Chemical & Biological Engineering, Center for Micro-Engineered Materials, University of New Mexico, Albuquerque, NM 87131, USA
[2] EWII Fuel Cells, LLC., 8500 Washington St. NE, B-1, Albuquerque, NM, 87113, USA
[3] Institut de Chimie et Procédés pour l'Energie, l'Environnement et la Santé, UMR 7515 CNRS-University of Strasbourg, Strasbourg Cedex, 67087, France
[4] Institut de Chimie de Strasbourg, UMR 7177 CNRS- University of Strasbourg, Strasbourg, 67070, France
[5] Boreskov Institute of Catalysis, Novosibirsk, 630090, Russia
[6] Department of Mechanical Engineering, Tufts University,200 College Avenue, Medford, MA 02155, USA
[7]Advanced Light Source, Lawrence Berkeley National Laboratory, 1 Cyclotron Road, Berkeley CA 94720, USA

1. Supplementary information related to electrochemical and electrocatalytic properties of NiMo/KB in 0.10 M NaOH

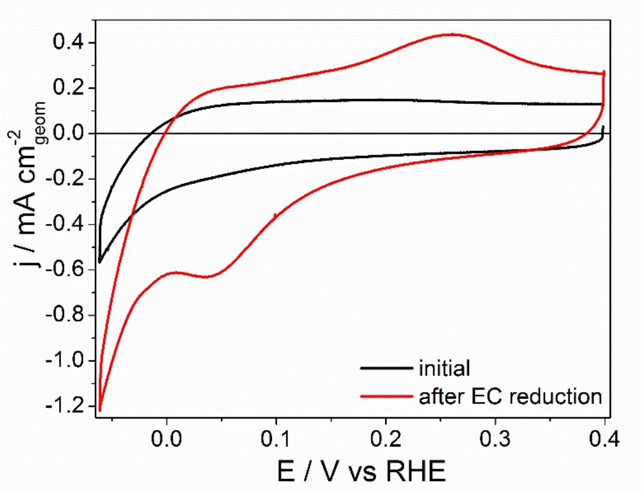

Figure S1. Cyclic voltammograms for initially immersed (black) and electrochemically reduced (red) NiMo/KB registered at 25 °C in N_2-saturated 0.10 M NaOH at v = 20 mV s^{-1}

Fig. S1 clearly shows the efficiency of the conditioning step in reducing the surface Ni oxide species by an increase of the currents corresponding to the formation/reduction of α-$Ni(OH)_2$. According to the Pourbaix diagram [1, 2], Mo in the potential interval studied is believed to be present in the form of either MoO_2 or MoO_4^{2-}. Note however, that Conway and Bai did not observe dissolution of Mo at high pH, suggesting slow dissolution kinetics [3]. We thus assume that MoO_2 /MoO_3 oxide species detected on the electrode surface by XPS are present on the electrode surface under the applied experimental conditions.

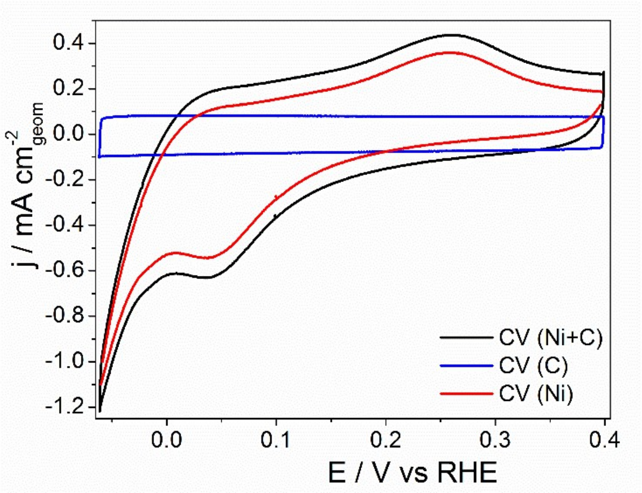

Figure S2. Cyclic voltammograms for NiMo/KB before (black) and after (red) subtraction of KB carbon registered at 25 °C in N_2-saturated 0.10 M NaOH at v = 20 mV s^{-1}

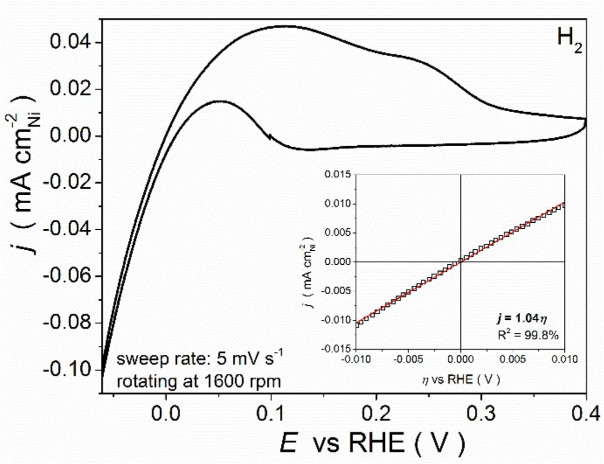

Figure S3. Cyclic voltammogram obtained for NiMo/KB (with a loading of 100 µg cm^{-2}) in H_2-saturated 0.1 M NaOH at a sweep rate of 5 mV s^{-1} and rotating speed of 1600 r.p.m. Inset demonstrates howthe exchange current density is calculated from the micropolarization region, according to the equation $j = \frac{j_0 nF}{RT}\eta$

2. Supplementary information related to the kinetic modeling of HOR/HER current-potential curves on NiMo/KB

The modelling of the experimental HOR/HER current potential curves was performed using Tafel-Heyrovsky-Volmer kinetic mechanism for the hydrogen electrode reactions and a two-steps mechanism for Nickel oxidation and reduction. In this work, the kinetic modelling allowed us the estimation of some important parameters such as the free energy of adsorption of the reaction intermediate (H_{ad}).

Equations for the HOR/HER modeling on Ni and NiMo

The hydrogen oxidation and evolution reactions in alkaline medium involves the Tafel (eq. 1) or the Heyrovsky (eq.2) step on free Ni sites:

$$H_2 + 2Ni \rightleftharpoons 2\ Ni\text{-}H_{ad} \tag{1}$$

$$H_2 + OH^- + Ni \rightleftharpoons Ni\text{-}H_{ad} + H_2O + e^- \tag{2}$$

The formation and oxidation of the adsorbed hydrogen intermediate H_{ad} can also occur according to the Volmer reaction in alkaline medium:

$$Ni\text{-}H_{ad} + OH^- \rightleftharpoons H_2O + e^- + Ni \tag{3}$$

The formation of $Ni\text{-}(OH)_2$ is modelled using a simplified two steps process:

$$OH^- + Ni \rightleftharpoons Ni\text{-}OH_{ad} + e^- \tag{4}$$

$$OH_{ad} + OH^- \rightleftharpoons Ni\text{-}(OH)_{2,ad} + e^- \tag{5}$$

The rates of steps (1)-(5) can be expressed as:

$$v_1 = k_1^0 S_t C_{H_2} (1 - \theta_H - \theta_{OH} - \theta_{(OH)_2})^2 - k_{-1}^0 S_t {\theta_H}^2 \tag{6}$$

$$v_2 = k_2^0 exp\left(\frac{(1-\alpha_2)FE}{RT}\right) C_{H_2} C_{OH^-} S_t (1 - \theta_H - \theta_{OH} - \theta_{(OH)_2}) - k_{-2}^0 exp\left(\frac{-\alpha_2 FE}{RT}\right) S_t \theta_H \tag{7}$$

$$v_3 = k_3^0 exp\left(\frac{(1-\alpha_3)FE}{RT}\right) S_t C_{OH^-} \theta_H - k_{-3}^0 exp\left(\frac{-\alpha_3 FE}{RT}\right) S_t (1 - \theta_H - \theta_{OH} - \theta_{(OH)_2}) \tag{8}$$

Here C_{H2}, and C_{OH-}, the concentrations of H_2 and OH^- respectively, are assumed to be the same in the bulk of the electrolyte and at the electrode surface. θ_H, θ_{OH}, $\theta_{(OH)2}$ are the surface coverage of the active intermediates: $Ni\text{-}H_{ad}$, $Ni\text{-}OH_{ad}$ and $Ni\text{-}(OH)_{2,ad}$ respectively. S_t is the mole number of active Ni sites per electrode geometric surface area. The meaning of the other symbols is explained in Table S1.

The rates of Ni-OH$_{ad}$ and Ni-(OH)$_{2,ad}$ formation/reduction in steps (4) and (5) are given by:

$$v_4 = k_4^0 exp\left(\frac{(1-\alpha_4)FE}{RT} - \frac{\gamma}{2}\theta_{OH}\right)C_{OH^-}S_t(1-\theta_H-\theta_{OH}-\theta_{(OH)_2}) - k_{-4}^0 exp\left(\frac{-\alpha_4 FE}{RT} + \frac{\gamma}{2}\theta_{OH}\right)S_t\theta_{OH} \tag{9}$$

$$v_5 = k_5^0 exp\left(\frac{(1-\alpha_5)FE}{RT}\right)C_{OH^-}S_t\theta_{OH} - k_{-5}^0 exp\left(\frac{-\alpha_5 FE}{RT}\right)S_t\theta_{(OH)_2} \tag{10}$$

where γ is the Frumkin interaction parameter used to improve the agreement between the experimental and the simulated curves. The repulsive interactions in the Ni-OH$_{ad}$ layer with γ=4 had to be introduced in the model for NiMo, while for Ni catalyst good agreement between experimental and simulated curves was obtained for γ=0 [4]. Note however that the consideration of slight repulsive interactions in the adlayer must be taken with caution, since the broadening of the Ni oxide formation peaks might also arise from a larger diversity of active sites in the NiMo/KB catalyst compared to Ni. The diversity of Ni active sites might also be the reason why the kinetic model fails to reproduce the magnitude of the second anodic peak at 0.25 V under H$_2$ atmosphere.

When the potential *E* is scanned at a sweep rate *v*, the current potential curves can be simulated by solving the following set of differential equations:

$$\frac{d\theta_H}{dt} = 2v_1 + v_2 - v_3 \tag{11}$$

$$\frac{d\theta_{OH}}{dt} = v_4 - v_5 \tag{12}$$

$$\frac{d\theta_{(OH)_2}}{dt} = v_5 \tag{13}$$

$$\frac{dE}{dt} = v \tag{14}$$

The total Faradaic current density then given by:

$$j_F = F(v_2 + v_3 + v_4 + v_5) \tag{15}$$

The set of rate constant used to simulate the current-potential curves on NiMo/KB are given in Table S1 and compared to a set that was able to reproduce the main features of the current potential curves obtained with pure metallic Ni1.

Table S1 List of parameters used for microkinetic simulations

Parameter	Meaning	Values	
		Ni_{pc}	NiMo/KB
C_{H2}	H_2 concentration	$7\ 10^{-4}$ M	$7\ 10^{-4}$ M
C_{OH-}	OH^- concentration	0.1 M	0.1 M
S_t	Surface active site density	$2.2\ 10^{-9}$ mol cm^{-2}	$2.0\ 10^{-8}$ mol cm^{-2}
α_2	Heyrovsky step charge transfer coefficient	0.4	0.4
α_3	Volmer step charge transfer coefficient	0.5	0.5
k_1^0	H_2 adsorption rate constant by the Tafel step	$3.94\ 10^7$ cm^3 s^{-1} mol^{-1}	$6.3\ 10^4$ cm^3 s^{-1} mol^{-1}
k_{-1}^0	H_2 formation rate constant by the Tafel step	0.010 s^{-1}	1 s^{-1}
k_2^0	H_2 adsorption rate constant by the Heyrovsky step	$8.8\ 10^9$ cm^6 s^{-1} mol^{-2}	$1.1\ 10^9$ cm^6 s^{-1} mol^{-2}
k_{-2}^0	H_2 desorption rate constant by the Heyrovsky step	0.016 s^{-1}	0.36 s^{-1}
k_{-3}^0	H_{ad} formation rate constant by the Volmer step	0.21 s^{-1} [1]	0.11 s^{-1} [2]
k_3^0	H_{ad} oxidation rate constant by the Volmer step	43 cm^3 s^{-1} mol^{-1} [1]a	$5.4\ 10^3$ cm^3 s^{-1} mol^{-1} [2]
k_4^0	Ni-OH_{ad} formation rate constant	$1.9\ 10^4$ cm^3 s^{-1} mol^{-1}	10^5 cm^3 s^{-1} mol^{-1}
k_{-4}^0	Ni-OH_{ad} reduction rate constant	19.3 s^{-1}	10 s^{-1}
E_4^0	Ni-OH_{ad} formation potential	0.06 V	0.0 V
k_5^0	Ni-$(OH)_{2,ad}$ formation rate constant	30 cm^3 s^{-1} mol^{-1}	11 cm^3 s^{-1} mol^{-1}
k_{-5}^0	Ni-$(OH)_{2,ad}$ reduction rate constant	3.3 s^{-1}	0.82 s^{-1}
E_5^0	Ni-$(OH)_{2,ad}$ formation potential	0.18 V	0.17 V
F	Faraday constant	96485 C mol^{-1}	96485 C mol^{-1}
R	Gas constant	8.314 J K^{-1} mol^{-1}	8.314 J K^{-1} mol^{-1}
T	Temperature	298 K	298 K
γ	Frumkin parameter	0	4

The rate constants k_4^0, k_{-4}^0, k_5^0, k_{-5}^0 were adjusted to simulate the Ni oxide formation/reduction peaks in the cyclic voltammograms of the NiMo/KB electrodes in N_2 purged solution and also the limitation of the HOR current due to the blocking of the Ni sites by oxide formation.

---

[1] These values of k_3^0 and k_{-3}^0 correspond to $\Delta_{ad}G^0 = -RT \ln(10000 * k_{-3}^0 / k_3^0) = -0.1$ eV.

[2] These values of k_3^0 and k_{-3}^0 correspond to $\Delta_{ad}G^0 = -RT \ln(10000 * k_{-3}^0 / k_3^0) = 0.04$ eV.

The values of k_1, k_2, k_3, k_{-1}, k_{-2}, and k_{-3} were adjusted to reproduce the level of the HOR/HER currents. However, it has to be mentioned that the exact values of these parameters cannot be determined by the fitting process due to the large number of unknown parameters.

With the parameters in Table S1, the simulated current-potential curves are in good agreement with the experimental ones in the potential range from -0.06 to 0.15V. The results of the kinetic modeling suggest a significant increase of the $\Delta_{ad}G^0$ from ca. -0.1 eV for polycrystalline Ni to 0.04 eV for the NiMo/KB catalyst, resulting in a strong increase of the HOR/HER currents. However, the fast kinetic of Ni-OH_{ad} and Ni-$(OH)_{2,ad}$ formation leads to the blocking of the Ni surface and the inhibition of the HOR current above 0.15V vs. RHE. Finally, the HOR switches from a predominant Heyrovsky-Volmer mechanism on the Ni electrode to a mixed Heyrovsky or Tafel-Volmer mechanism on the NiMo catalyst. However, further studies are required to determine the contribution of the Tafel and Heyrovsky processes in the HOR/HER currents.

3. Supplementary information on Synchrotron X-ray Computed Tomography

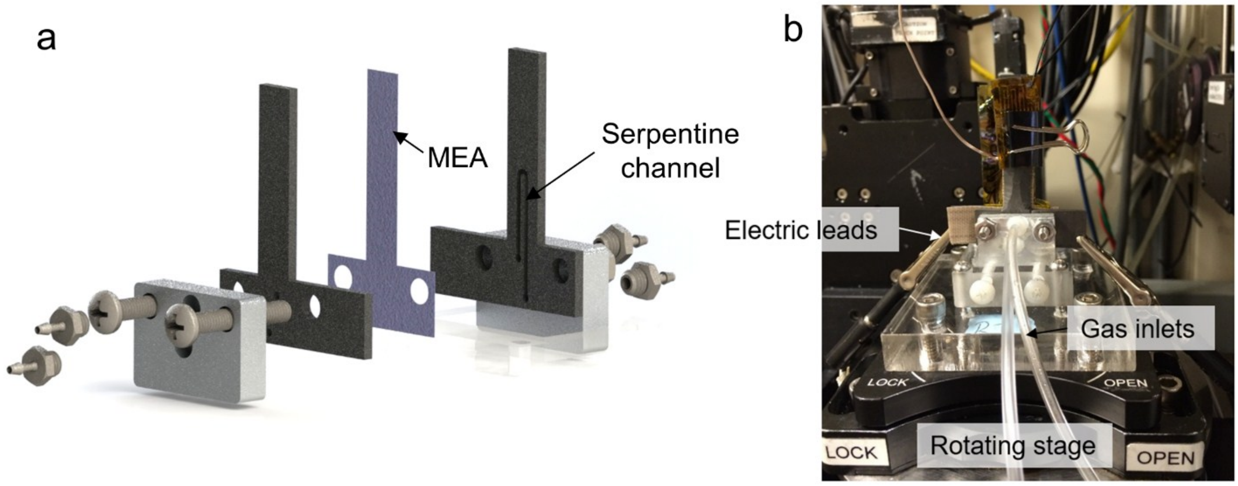

Figure S4. a) An expanded view of a sample-holder for in-operando experiments, b) sample holder mounted on the ALS Beamline 8.3.2 stage, where gas-lines and electric leads are shown too.

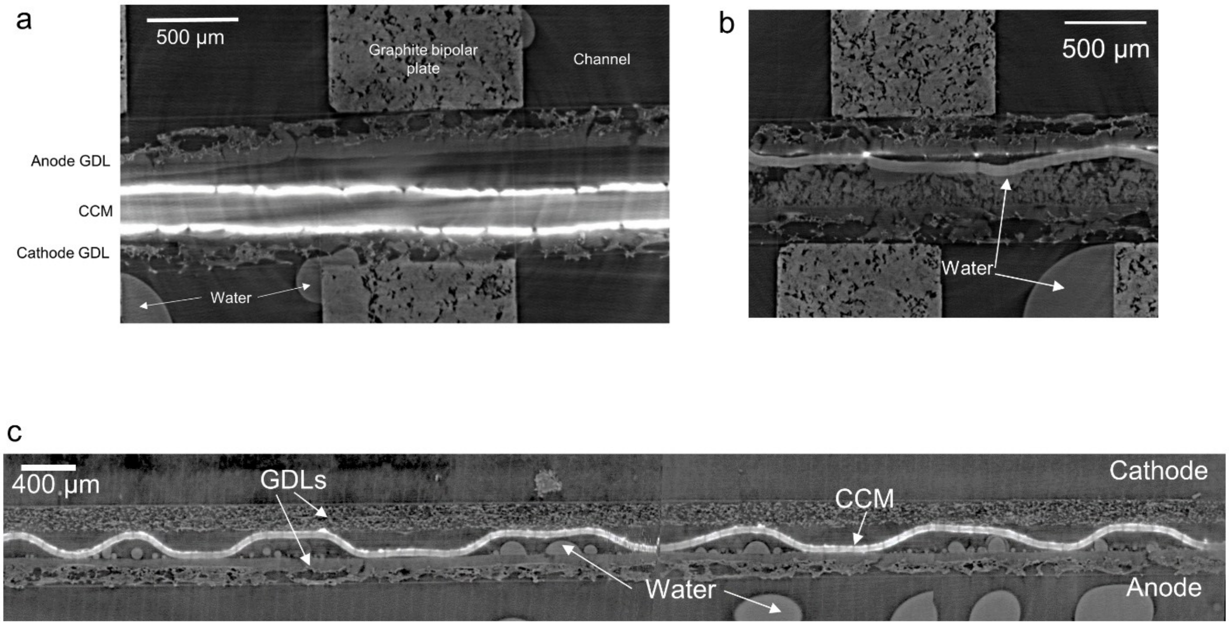

Figure S5. a) A cross-section tomograph of PEMFC with PGM MEA operating at 50 mA cm^{-2} and 100% RH, T = 30^oC, H_2/Air b) a cross-section tomograph of PGM-free cathode PEMFC operating at 30 mA cm^{-2}, 100% RH, T = 30^oC, H_2/air, and c) along-the-channel cross-section tomograph of PGM AEMFC at 30 mA/cm^2, 100% RH, T = 30^oC, H_2/O_2.

Video S1. A sliding view of cross-section tomographs along the full length of channel and land, where the top is anode and the bottom is cathode. The brighter cracked region is anode catalyst layer.

Video S2. A rotating view of cross-section slides of the same sample presented in Video S1.

4. Supplementary information on X-Ray Photoelectron Spectroscopy

Ni 2p spectra were fitted using synthetic shapes created for Ni metal, NiO and $Ni(OH)_2$ developed by Biesinger et al. [29] The positions and ratios between all peaks for each type of nickel were fixed to create the photoelectron synthetic shapes that were used to fit the experimental spectra. Two peaks for mixed nickel molybdenum oxide $NiMoO_x$ at positions reported in the literature were added to complete the curve-fit. When anode was separated for analysis from the MEA after test, thin layer GDE was left, which resulted in fluorine contributing to very surface sensitive XPS analysis. F KLL Auger peak contributes into the region where Ni 2p is detected. For Ni 2p spectra acquired from MEAs, two wide peaks coming from F KLL Auger contribution were added to complete the fit. Mo 3d spectra were fitted using doublet for each type of molybdenum state. The separation between 5/2 and 3/2 parts of spin-orbit splitting in Mo 3d orbital is 3.16 eV, and the ratio of peaks is 4 to 3. Four peaks at positions reported in the literature due to metallic Mo, Mo (IV) oxide, Mo (V) and mixed nickel alloy oxide were used to fit the spectrum of fresh catalyst.

Table S2. Elemental composition (in at %) and relative chemical composition for Ni 2p and Mo 3d spectra

Sample	C 1s	O 1s	Ni 2p	Mo 3d	N 1s	Ni/Mo
Catalyst	91.3	7.1	0.64	0.92		*0.7*
MEA fresh	94.1	4.6	0.24	0.47	0.6	*0.5*
MEA AT	90.3	7.7	0.92	0.06	1.0	*16.4*

	Mo	MoO2	Mo(V)	NiMoOx	MoO3	Ni metal	NiO	Ni(OH)2	NiMoOx
Catalyst	2.4	13.2	26.2	58.2		19.0	30.2	39.2	11.4
Fresh MEA				46.4	53.6	19.9	48.0	11.3	20.6
MEA AT 2				41.1	58.9	0.0	16.1	82.0	1.9

In fresh catalyst, Mo exists in multiple chemical forms - from a small amount of metallic Mo to major component being mixed nickel molybdenum oxide. Ni is present as a mixture of metallic Ni, Ni oxides, hydroxide and mixed nickel molybdenum oxide $NiMoO_x$. In the catalyst, the peak due to the mixed oxide $NiMoO_x$ in Ni 2p spectrum occupies 11 % of the total Ni present. The peak due to the same mixed oxide $NiMoO_x$ from Mo 3d spectrum shows 60% of total Mo present. This difference is due to the contribution of MoO_3 into the same peak.

5. Supplementary information on *in situ* studies

Figure S6 shows O 1s spectra in three environments, i.e. UHV, 75 mbar in H_2 and equal pressure of 75 mbar of H_2 and H_2O. O1s spectrum in UHV was fitted with three peaks for Ni-KB catalyst and two peaks for NiMo-KB catalyst. The ratio of peaks and positions have been fixed to the largest peak, which is at 532.6 eV for Ni-KB and 531.7 for NiMo catalyst. This constraint spectral shape representing oxygen present in UHV was used in fitting the spectra obtained in hydrogen and mixture of water and hydrogen. As expected in hydrogen, no change in oxygen speciation is observed. In a mixture of hydrogen and water, a large peak due to water is present at the highest binding energy. In addition to that, the small peak due to adsorbed -OH needs to be added to complete curve fit. This peak is quite small in comparison to other oxygen species present, so the contribution of -OH bound to the surface of the catalyst is expected to be small.

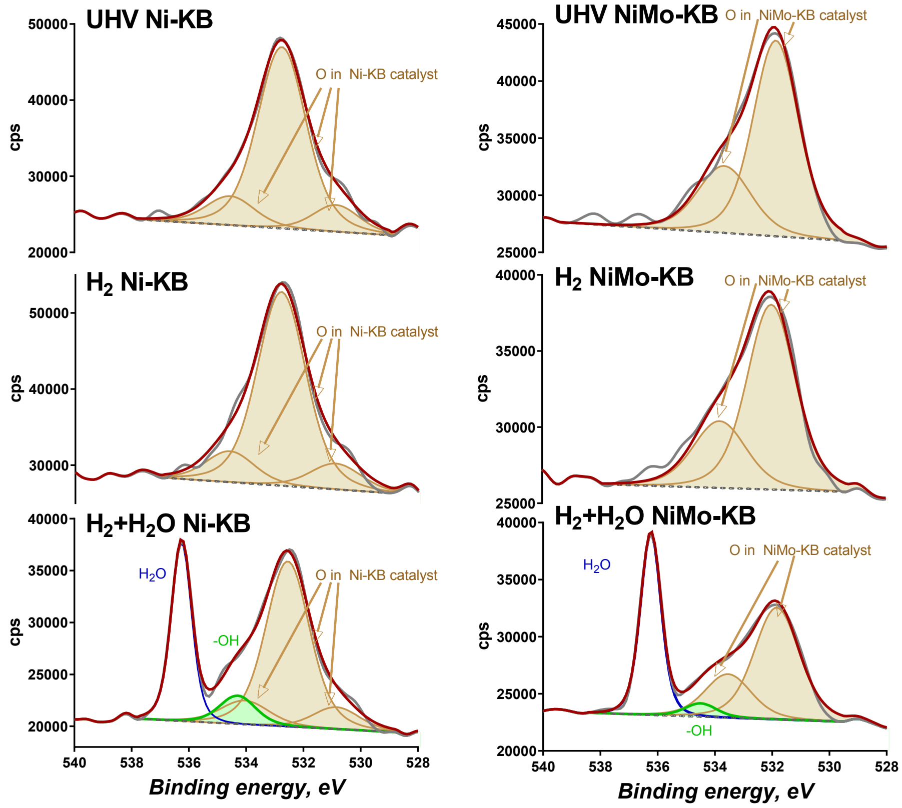

Figure S6. High resolution O 1s spectra in UHV, H_2 and mixture of H_2 and water at 70°C for Ni-KB and NiMo-KB catalysts.

[1] Takeno, N. Atlas of Eh-pH diagrams Intercomparison of thermodynamic databases. *National Institute of Advanced Industrial Science and Technology* (2005).

[2] P.A. Nikolaychuk , A.G. Tyurin, The Revised Pourbaix Diagram for Molybdenum, Butlerov Communications 24 (2011) 101-105.

[3] B.E. Conway, L. Bai, Determination of the adsorption behaviour of “overpotential-deposited” hydrogen-atom species in the cathodic hydrogen-evolution reaction by analysis of potential-relaxation transients, J. Chem. Soc. Faraday Trans. 1 Phys. Chem. Condens. Phases. 81 (1985) 1841–1862.

[4] A. G. Oshchepkov, A. Bonnefont, V. A. Saveleva, V. Papaefthimiou, S. Zafeiratos, S. N. Pronkin, V. N. Parmon, E. R. Savinova "Exploring the Influence of the Nickel Oxide Species on the Kinetics of Hydrogen Electrode Reactions in Alkaline Media." Topics in Catalysis 59 (2016) 1319-1331.